Onsager's cross coupling effects in gas flows confined to micro-channels

Ruijie Wang,[1,2] Xinpeng Xu,[2] Kun Xu,[2] and Tiezheng Qian[2,*]

[1]*School of Power and Energy, Northwestern Polytechnical University, Xi'an 710072, Shaanxi, P.R. China*

[2]*Department of Mathematics, Hong Kong University of Science and Technology, Clear Water Bay, Kowloon, Hong Kong*

(Received 23 February 2016; published 18 August 2016)

In rarefied gases, mass and heat transport processes interfere with each other, leading to the mechano-caloric effect and thermo-osmotic effect, which are of interest to both theoretical study and practical applications. We employ the unified gas-kinetic scheme to investigate these cross coupling effects in gas flows in micro-channels. Our numerical simulations cover channels of planar surfaces and also channels of ratchet surfaces, with Onsager's reciprocal relation verified for both cases. For channels of planar surfaces, simulations are performed in a wide range of Knudsen number, and our numerical results show good agreement with the literature results. For channels of ratchet surfaces, simulations are performed for both the slip and transition regimes, and our numerical results not only confirm the theoretical prediction [Phys. Rev. Lett. **107**, 164502 (2011)] for the Knudsen number in the slip regime but also show that the off-diagonal kinetic coefficients for cross coupling effects are maximized at a Knudsen number in the transition regime. Finally, a preliminary optimization study is carried out for the geometry of Knudsen pump based on channels of ratchet surfaces.

DOI: 10.1103/PhysRevFluids.1.044102

I. INTRODUCTION

Onsager's reciprocal relations for linear irreversible processes [1,2] play a crucial and important role in the theory of nonequilibrium thermodynamics. The kinetics of gases can be described by elementary processes of molecular collisions where microscopic reversibility and detailed balance are preserved. For systems slightly deviating from equilibrium, the linear response theory applies and Onsager's reciprocal relations can be derived with the regression hypothesis [1]. Typical examples in gas flows are the cross coupling between mass and heat diffusion in a multicomponent gas [3], and the mechano-caloric effect and thermo-osmotic effect in a single-component gas [4]. The latter one not only provides an interesting case for theoretical study but also has practical applications in micro-devices [5,6].

Waldmann [4] studied the cross coupling effect in channels of parallel planar surfaces in both the free molecular ($\mathrm{Kn} \geqslant 10$) and slip ($0.001 \leqslant \mathrm{Kn} \leqslant 0.1$) regimes, and de Groot and Mazur [7] studied the reciprocal relations for general discontinuous systems. Loyalka [8,9] and Sharipov [10] analyzed the cross coupling effect by means of the linearized Boltzmann method and obtained the coupling coefficients. The theoretical analysis of Loyalka [8] is valid for capillaries of arbitrary shape, and there have been many works, including numerical calculations, devoted to capillaries of planar surfaces and various shapes of the cross section [9,11–14]. The thermo-osmotic effect has attracted much attention recently since it can be used to design pumping devices without any moving part, i.e., the Knudsen pump [5]. In addition to the earlier proposed Knudsen pump [5,6], capillaries with ratchet surfaces have the potential for other possible configurations [15]. The driving mechanism of these systems has been analyzed by Wüger [15] as well as Hardt *et al.* [16], and the mass and momentum transfer has been studied by Donkov *et al.* [17].

*Corresponding author: maqian@ust.hk

In the present work, we will study the cross coupling phenomena for a long capillary by using the unified gas-kinetic scheme [18,19]. We will study the case of planar surfaces as well as the case of ratchet surfaces. The cross coupling mechanism will be presented for both cases. The coupling coefficients for the case of planar surfaces are numerically calculated and compared to literature results. The coupling coefficients for the case of ratchet surfaces are numerically calculated and analyzed, with a comparison to literature results as well. A preliminary geometry optimization for the design of Knudsen pump is also presented.

In our simulations for the case of ratchet surfaces, a channel of finite length is used with the pressure boundary condition applied at the two ends. In the presence of both pressure difference and temperature difference, the cross coupling effects, namely the mechano-caloric effect and thermo-osmotic effect, can be jointly studied to reveal the underlying reciprocal symmetry. However, with the periodic boundary condition used by Donkov *et al.* [17], only the thermo-osmotic effect is attainable because no pressure difference can be applied to generate the mechano-caloric effect. The numerical scheme used in the present work is applicable for all Knudsen numbers, and this allows us to study the cross coupling phenomena beyond the slip regime in which Wüger's theory [15] is valid. In particular, we find that the cross coupling effects are maximized at a Knudsen number in the transition regime.

II. CROSS-COUPLING IN GAS FLOWS IN MICRO-CHANNELS

In a closed system out of equilibrium, the rate of entropy production can be expressed as

$$\frac{dS}{dt} = \sum_{i=1}^{N} J_i X_i, \tag{1}$$

where S is the entropy, J_i are the thermodynamic fluxes, and X_i are the conjugate thermodynamic forces. For small deviation away from equilibrium, we have the linear relations between J_i and X_i:

$$J_i = \sum_{j=1}^{N} L_{ij} X_j, \tag{2}$$

where L_{ij} are the kinetic coefficients.

Onsager's reciprocal relations states that $L_{ij} = \epsilon_i \epsilon_j L_{ji}$ as a result of microscopic reversibility [1,2,10,20], where $\epsilon_i = \pm 1$ depending on whether X_i changes its sign via the time reversal [10]. For the situations considered here, we have $L_{ij} = L_{ji}$. Starting from the Gibbs equation, the thermodynamic fluxes and forces can be identified for gas flows, and the corresponding constitutive equations can be derived [3], with the explicit expression of the kinetic coefficients [8,9,21,22].

A. Micro-channels of planar surfaces

A schematic illustration of the cross coupling in a channel of planar surfaces can be found in Fig. 1, where a long channel is confined by two parallel solid plates separated by a distance H

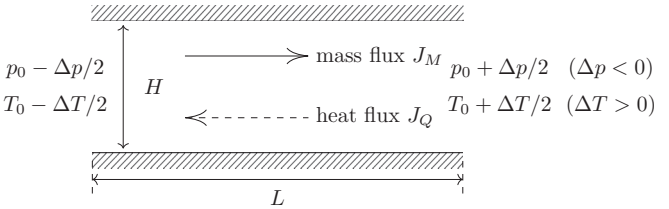

FIG. 1. A schematic illustration of the cross coupling in a channel of planar surfaces.

and connected with two reservoirs. The left reservoir is maintained at pressure $p_0 - \Delta p/2$ and temperature $T_0 - \Delta T/2$ while the right reservoir is maintained at $p_0 + \Delta p/2$ and $T_0 + \Delta T/2$. We use $\Delta p < 0$ and $\Delta T > 0$ in our simulations, with $|\Delta p/p_0| \ll 1$ and $|\Delta T/T_0| \ll 1$ to ensure the linear response. Usually, a mass flux to the right is generated by the pressure gradient due to $\Delta p < 0$, and a heat flux to the left is generated by the temperature gradient due to $\Delta T > 0$. For rarefied gas, however, Δp also contributes to the heat flux and ΔT also contributes to the mass flux. These cross coupling effects are called the mechano-caloric effect and thermo-osmotic effect respectively.

For a single-component gas, the rate of entropy production can be expressed as [4]

$$\frac{dS}{dt} = J_M \Delta\left(-\frac{\nu}{T}\right) + J_E \Delta\left(\frac{1}{T}\right), \tag{3}$$

where ν is the chemical potential per unit mass, J_E and J_M are the energy flux and mass flux from the left reservoir to the right reservoir, and Δ means the quantity on the right minus the quantity on the left. Here ν and J_E can be written as

$$\nu = h - Ts, \tag{4}$$

$$J_E = J_Q + hJ_M, \tag{5}$$

where s and h are the entropy and enthalpy per unit mass, and J_Q is the heat flux. Together with the Gibbs-Duhem equation

$$d\nu = -sdT + dp/\rho, \tag{6}$$

where ρ is the mass density, Eq. (3) becomes

$$\frac{dS}{dt} = -\frac{1}{\rho T} J_M \Delta p - \frac{1}{T^2} J_Q \Delta T. \tag{7}$$

According to Eq. (7), the thermodynamic forces and fluxes are connected in the form

$$\begin{bmatrix} J_M \\ J_Q \end{bmatrix} = \begin{bmatrix} L_{MM} & L_{MQ} \\ L_{QM} & L_{QQ} \end{bmatrix} \begin{bmatrix} -\rho_0^{-1} T_0^{-1} \Delta p \\ -T_0^{-2} \Delta T \end{bmatrix}, \tag{8}$$

with

$$L_{MQ} = L_{QM}, \tag{9}$$

due to Onsager's reciprocal relations. The detailed mechanism may vary with geometric configuration and rarefaction. Here and throughout the paper, the subscript "0" denotes the reference state from which various deviations (in pressure, temperature, etc.) are measured.

In the free molecular regime and with specular reflection on plates, the gas molecules travel ballistically from on side to the other, and the distribution function at any point can be treated as a combination of two half-space Maxwellians from the two reservoirs. The kinetic coefficients in Eq. (8) can be analytically derived in this case [4], given by

$$\begin{bmatrix} L_{MM} & L_{MQ} \\ L_{QM} & L_{QQ} \end{bmatrix} = \frac{H\rho_0 T_0}{4} \sqrt{\frac{8k_B T_0}{\pi m}} \begin{bmatrix} \rho_0/p_0 & -1/2 \\ -1/2 & 9p_0/4\rho_0 \end{bmatrix}, \tag{10}$$

where k_B is the Boltzmann constant and m is the molecular mass.

If the temperature gradient is imposed on the plates and the gas molecules are diffusely reflected, then the mass flux due to the temperature gradient is generated by thermal creep on the plates [5,7,23]. The kinetic coefficients in this case have been calculated by several authors using different methods [11]. Assuming the length to height ratio of the channel is fixed and noting $\rho\lambda = \text{const}$ and $\mu \propto T^{1/2}$ for hard-sphere molecules, the average velocity $\overline{U}$ induced by thermal creep can be

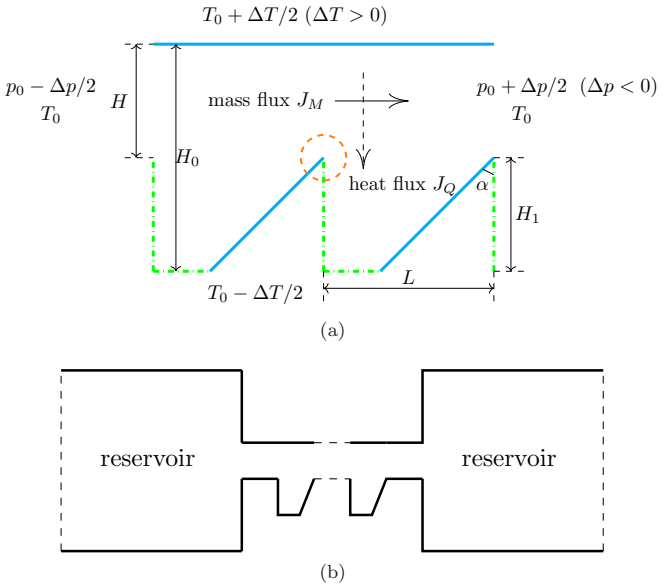

FIG. 2. A schematic illustration of the cross coupling in a channel of ratchet surfaces. (a) Two blocks of a channel of ratchet surfaces. The upper wall and the lower tilted walls (blue solid lines) are diffusely reflective. The lower horizontal and vertical walls (green dot-dashed lines) are specularly reflective. (b) Simulation geometry with multiple blocks in the channel.

estimated from the Maxwell slip boundary condition [23],

$$\overline{U} \sim \frac{\mu_0}{\rho_0 T_0} \nabla T \propto \mathrm{Kn} \frac{\Delta T}{\sqrt{T_0}}, \tag{11}$$

where μ is the dynamic viscosity independent of the density, λ is the mean free path given by

$$\lambda = \frac{16}{5} \left(\frac{m}{2\pi k_B T} \right)^{1/2} \frac{\mu}{\rho},$$

and $\mathrm{Kn} = \lambda_0 / H$ is the Knudsen number. Rigorous expressions of $\overline{U}$ can be found in Refs. [11,12], but an approximate expression is enough to serve our purpose here. In later sections, we will show that L_{MQ} and L_{QM} are equal and increase with the increasing Kn in our simulations to validate our numerical scheme.

B. Micro-channels of ratchet surfaces

The mechanism for the cross coupling in a channel of ratchet surfaces is more complicated. Consider a long channel consisting of repeating structure [17] as shown in Fig. 2(a), where the two ends are connected to two reservoirs maintained at $(p_0 - \Delta p/2, T_0)$ on the left and $(p_0 + \Delta p/2, T_0)$ on the right with $\Delta p < 0$. The upper wall (blue solid lines) is diffusely reflective and maintained at $T_0 + \Delta T/2$ with $\Delta T > 0$, and the lower tilted walls (blue solid lines) are diffusely reflective and maintained at $T_0 - \Delta T/2$. The lower horizontal and vertical walls (green dot-dashed lines) are specularly reflective. Usually, a mass flux from the left to the right is generated by the pressure gradient due to $\Delta p < 0$, and a heat flux from the top to the bottom is generated by the temperature gradient due to $\Delta T > 0$. For rarefied gas, however, Δp also contributes to the vertical heat flux, and ΔT also contributes to the horizontal mass flux. Our simulations are carried out for $|\Delta p / p_0| \ll 1$ and $|\Delta T / T_0| \ll 1$ to ensure the linear response.

In general, a temperature difference can also be applied in the horizontal direction, and a heat flux can also exist in this direction as the conjugate flux. This means that there are three thermodynamic forces (i.e., the pressure difference in the horizontal direction, the temperature difference in the horizontal direction, and the temperature difference in the vertical direction) and their conjugate fluxes. In the present study, we set the temperature difference in the horizontal direction to be zero. We also ignore the heat flux in the horizontal direction (although it may well exist). The rate of entropy production associated with the vertical temperature difference ΔT is given by $-T^{-2}J_Q\Delta T$. As a result, the two thermodynamic forces and their conjugate fluxes under consideration are connected in the form

$$\begin{bmatrix} J_M \\ J_Q \end{bmatrix} = \begin{bmatrix} L_{MM} & L_{MQ} \\ L_{QM} & L_{QQ} \end{bmatrix} \begin{bmatrix} -\rho_0^{-1}T_0^{-1}\Delta p \\ -T_0^{-2}\Delta T \end{bmatrix}, \tag{12}$$

with

$$L_{MQ} = L_{QM}, \tag{13}$$

due to Onsager's reciprocal relations. Here J_M is the *horizontal* mass flux (from the left to the right) and J_Q is the *vertical* heat flux (from the bottom to the top).

Since the upper wall and the lower tilted walls are maintained at different temperatures (with $\Delta T > 0$), the isothermal lines near the tips of the tilted walls (indicated by a red dashed circle) are sharply curved and a thermal edge flow is induced at the tip from the top to the bottom [5,16]. It is possible to make a rough estimation of the induced flow velocity at the tip [5,15]. If all the walls are assumed to be diffusely reflective, then the temperature gradient along the tilted wall near the tip is approximated by

$$\nabla_{||}T = \Delta T \frac{\pi^2}{(2\pi-\alpha)^2}\cos\left(\frac{\alpha}{2}\right)\frac{H^{-\pi/(2\pi-\alpha)}}{\lambda_0^{1-\pi/(2\pi-\alpha)}}, \tag{14}$$

where λ_0 is the mean free path at (p_0,T_0) [15]. Here Eq. (14) is valid only in the hydrodynamic regime due to the assumption that the temperature obeys the Laplace equation [15]. However, it can still provide an approximate but very useful description for the slip regime. By use of $\rho\lambda = \text{const}$ and $\mu \propto T^{1/2}$ for hard-sphere molecules, the induced velocity in the slip regime can be estimated from the slip boundary condition [23]:

$$\overline{U} \sim \frac{\mu_0}{\rho_0 T_0}\nabla_{||}T \propto \frac{\Delta T}{\sqrt{T_0}}\frac{1}{(2\pi-\alpha)^2}\cos\left(\frac{\alpha}{2}\right)\left(\frac{\lambda_0}{H}\right)^{\pi/(2\pi-\alpha)}. \tag{15}$$

For $0 \leqslant \alpha < \pi/2$ and $\mathrm{Kn} = \lambda_0/H \leqslant 0.1$ in the slip regime, the induced velocity is

(1) Proportional to ΔT
(2) A decreasing function of T_0
(3) A decreasing function of α because a smaller α means sharper edges
(4) An increasing function of Kn because a larger Kn leads to stronger nonequilibrium effect.

It is worth noting that $\overline{U}$ will decrease if the Knudsen number exceeds a certain value since the thermally induced flows are typically strongest in the lower transition regime (where the Knudsen number is slightly higher than that in the slip regime) [5]. According to Eq. (15), the average velocity for the current configuration is assumed to have the form

$$\overline{U} \propto \mathrm{Kn}^{C_2}\frac{\Delta T}{\sqrt{T_0}}, \tag{16}$$

where C_2 is a constant determined by a specific geometry.

In later sections, we will show that L_{MQ} and L_{QM} are equal in our simulations, and C_2 determined from simulations according to Eq. (16) is very close to the exponent predicted by Eq. (15).

III. NUMERICAL RESULTS AND DISCUSSION

The kinetic coefficients are to be calculated and presented in dimensionless form as

$$\hat{L}_{MQ} = -L_{MQ}\left(\frac{2k_B}{m\rho_0 C_0^3 H}\right), \quad \hat{L}_{QM} = -L_{QM}\left(\frac{2k_B}{m\rho_0 C_0^3 H}\right), \tag{17}$$

where ρ_0 and T_0 are the density and temperature of the reference state, $C_0 = \sqrt{2k_B T_0/m}$ is the most probable speed, and H is the height of the channel to define the Knudsen number $\mathrm{Kn} = \lambda_0/H$. The mean free path in the reference state is λ_0. The above normalization makes it easier to compare our results with the benchmark solutions, and the normalized coefficients can reflect the mechanism more directly as shown below.

As the density variation is small in the simulation, the mass flux can be expressed as

$$J_M \approx \rho_0 \overline{U} H. \tag{18}$$

Assuming that there is no pressure difference, we have

$$\rho_0 \overline{U} H = \hat{L}_{MQ}\left(\frac{m\rho_0 C_0^3 H}{2k_B}\right)\frac{\Delta T}{T_0^2}, \tag{19}$$

which leads to

$$\overline{U} = \hat{L}_{MQ} C_0 \frac{\Delta T}{T_0} \propto \hat{L}_{MQ}\frac{\Delta T}{\sqrt{T_0}}. \tag{20}$$

Through a comparison of Eq. (20) with Eqs. (11) and (16), the dimensionless $\hat{L}_{MQ}$ is expected to have the form

$$\hat{L}_{MQ} = C_1 \mathrm{Kn}^{C_2}, \tag{21}$$

where C_1 and C_2 are constants determined by a specific geometry. They are to be obtained by fitting the simulation data.

For the cross coupling considered here, two thermodynamic fluxes (mass flux and heat flux) and the corresponding forces (pressure difference and temperature difference) can be directly extracted from the simulation data in a single simulation. In order to determine all the kinetic coefficients, simulations need to be performed (at least) twice with different Δp and ΔT for the same system (with the same geometry and the same Knudsen number). We add that although the simulation method described in the Appendix uses the BGK-type equation which is nonlinear, very small Δp and ΔT were used in our simulations in order to ensure that dynamics is slow and hence linear response is valid.

A. Cross coupling in channels of planar surfaces

First we calculate the kinetic coefficients for channels with planar surfaces and compare our results with those in literature [11,24,26]. A schematic illustration for the simulation geometry can be found in Fig. 1. The solid surfaces are diffusely reflective and have linearly distributed temperature from $T_0 - \Delta T/2$ to $T_0 + \Delta T/2$. The gas particles are hard-sphere and monatomic, with the Prandtl number $\mathrm{Pr} = 2/3$ and the dynamic viscosity $\mu \propto T^{0.5}$. The Knudsen number is defined as $\mathrm{Kn} = \lambda_0/H$. Δp and ΔT are kept small enough so that the response of fluxes to forces is linear. The length to height ratio of the channel is taken to be 20 in order to reduce the influence of inlet and outlet. When extracting the kinetic coefficients, the pressure and temperature differences are measured at the inlet and outlet, the mass flux J_M is measured over the cross section at the inlet and outlet, and the heat flux J_Q is measured over the cross section in the middle of the channel. This is slightly different from the expressions given by Ref. [22], where the mass flux and heat flux are both measured at the open boundaries of the channel. We didn't choose the open boundaries to measure the heat flux because of the following. (1) Ideally, if the flow is a fully developed steady-state flow

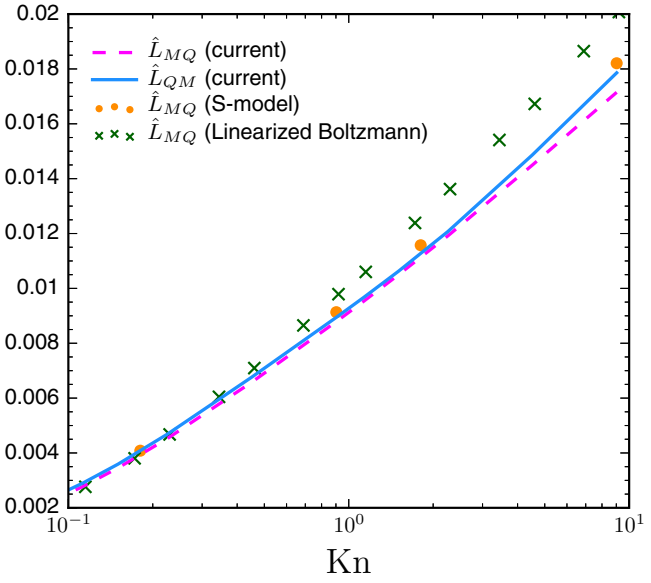

FIG. 3. The normalized off-diagonal coefficients $\hat{L}_{MQ}$ and $\hat{L}_{QM}$ versus the Knudsen number. The two references are the S-model solution based on the variational method by Chernyak *et al.* [24] and the linearized Boltzmann solution by Ohwada *et al.* [25].

(e.g., in an infinitely long channel), then the heat flux is uniform along the channel. (2) However, in our simulations, the flow field variables are greatly influenced by the inlet and outlet effect. Therefore measuring the heat flux in the middle of the channel is easier and more practical.

Figure 3 shows the normalized off-diagonal coefficients $\hat{L}_{MQ}$ and $\hat{L}_{QM}$ versus the Knudsen number. In our simulations, we have tried to double the grid, the channel length, and the reservoir size, and the extracted kinetic coefficients showed very little change. The two coefficients are very close to each other with a relative difference less than 5% and have good agreement with the S-model solution based on the variational method by Chernyak *et al.* [24]. The linearized Boltzmann results [25] start to show appreciable deviation from our numerical results at Kn ≈ 1 and the deviation increases with the increasing Kn. We would like to point out that both reference solutions are for channels of infinite length, while our simulations used $L/H = 20$. The difference between the S-model and the linearized Boltzmann equation in collision term would lead to some discrepancy for long channels. The finite channel length used in our simulations may contribute to the deviation noted in Fig. 3 as well. The off-diagonal coefficients are zero at Kn $= 0$ since there is no thermally induced flow in the continuum limit and the heat flux simply follows Fourier's law. The normalized coefficients increase with the increasing Knudsen number. In the slip regime ($0.001 <$ Kn < 0.1), $\hat{L}_{MQ} \sim$ Kn, while at large Knudsen numbers (Kn > 3), the profile is almost linear, which means $\hat{L}_{MQ} = \hat{L}_{QM} \sim \log(\text{Kn})$. This agrees with the conclusion obtained from linearized Boltzmann equation for two-dimensional infinitely long channels [11,26].

B. Cross coupling in channels of ratchet surfaces

In our simulations, each channel consists of seven repeating blocks as shown in Fig. 2(a), and each block has $L/H_0 = 1$, $H_1/H = 1$, and $\alpha = 45^\circ$. In addition, two parallel sections with specularly reflective walls of length L are attached at the two ends. The channel is then connected to two reservoirs. A schematic illustration for the whole system is shown in Fig. 2(b). The parallel sections with specularly reflective walls connected to the reservoirs are introduced to reduce the boundary effect of the inlet and outlet on the ratchet sections and to simplify the measurement of mass flux.

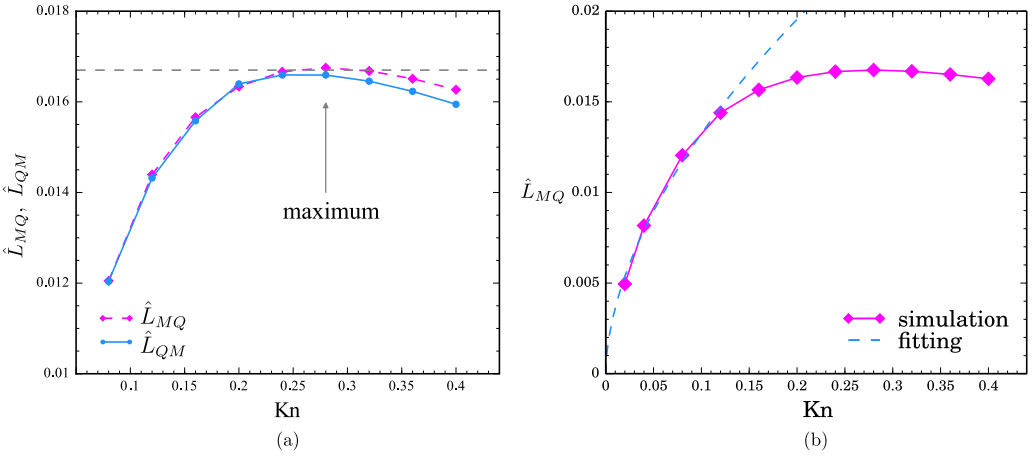

FIG. 4. (a) The normalized off-diagonal coefficients $\hat{L}_{MQ}$ and $\hat{L}_{QM}$ versus the Knudsen number. The dashed line is used to indicate that $\hat{L}_{MQ}$ and $\hat{L}_{QM}$ both exhibit their maxima at Kn ≈ 0.28. (b) $\hat{L}_{MQ}$ from simulations. For Kn $\leqslant 0.12$, the data fitting gives $\hat{L}_{MQ} = 0.0483\text{Kn}^{0.562}$, represented by the dashed line.

The gas particles are still hard-sphere and monatomic, with the Prandtl number $\text{Pr} = 2/3$ and the dynamic viscosity $\mu \propto T^{0.5}$. The Knudsen number is defined as $\text{Kn} = \lambda_0/H$. When extracting the kinetic coefficients, the pressure difference is measured at the inlet and outlet, the mass flux J_M is measured over the cross section at the inlet and outlet, and the heat flux J_Q is measured over all the lower tilted walls.

Figure 4(a) shows the normalized off-diagonal coefficients $\hat{L}_{MQ}$ and $\hat{L}_{QM}$ versus the Knudsen number. The two coefficients are very close to each other with a relative difference less than 2%, indicating that the relation $L_{MQ} = L_{QM}$ is well satisfied in our simulations. The off-diagonal coefficients are zero at $\text{Kn} = 0$ since there is no thermally induced flow in the continuum limit and the heat flux simply follows Fourier's law. As the Knudsen number increases from zero, the rarefaction effects begin to emerge at the sharp edge of the ratchet and lead to nonzero $\hat{L}_{MQ}$ and $\hat{L}_{QM}$. It is further noted that $\hat{L}_{MQ}$ and $\hat{L}_{QM}$ both exhibit their maxima at Kn ≈ 0.28. This value of Kn (in the transition regime) is consistent with the results for $\hat{L}_{MQ}$ in Ref. [17] for a similar ratchet geometry with periodic boundary condition. Physically, the cross coupling effects arise from the thermally induced flow, which is the strongest at the sharp edge. As the Knudsen number becomes higher than a certain value, the surface structure is no longer clearly detectable by the particles, and hence the off-diagonal coefficients will decrease with the increasing Knudsen number. From the distinct behaviors of $\hat{L}_{MQ}$ as a function of Kn in the slip and transition regimes, a maximum is expected for $\hat{L}_{MQ}$.

Now we perform the data fitting according to $L_{MQ} = L_{QM}$ and Eq. (21). Since this formula is valid in the slip regime ($0.001 \leqslant \text{Kn} \leqslant 0.1$), two additional simulations are carried out to obtain $\hat{L}_{MQ}$ at $\text{Kn} = 0.02$ and 0.04, as shown in Fig. 4(b). The data fitting uses only the first four data points (for $\text{Kn} \leqslant 0.12$, see Fig. 4(b)) and gives

$$\hat{L}_{MQ} = 0.0483\text{Kn}^{0.562}. \tag{22}$$

Inserting $\alpha = \pi/4$ into Eq. (15), we find

$$\bar{U} \propto \text{Kn}^{4/7}, \tag{23}$$

in which the exponent $4/7 \simeq 0.571$ is very close to the fitting parameter 0.562 in Eq. (22). Physically, the exponent C_2 directly reflects the underlying cross coupling mechanism, and therefore our simulation results have confirmed the theory proposed in Ref. [15] for Kn in the slip regime.

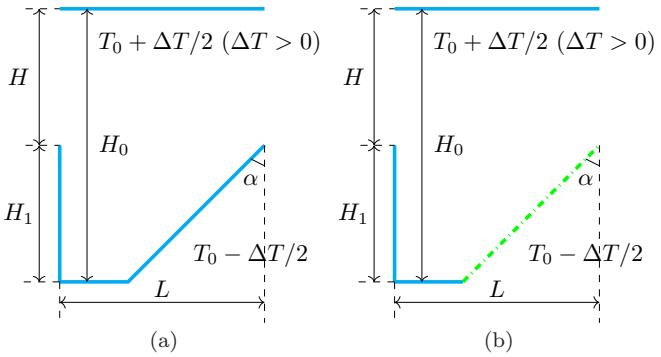

FIG. 5. (a) The diffuse configuration. (b) The diffuse-specular configuration.

IV. KNUDSEN PUMP

Wüger [15] and Donkov *et al.* [17] have proposed the capillary with ratchet surfaces as another possible configuration for the Knudsen pump. In this section, a preliminary optimization study is provided for this purpose. For accuracy and simplicity, only one block is used in the simulations here, and the inlet and outlet are replaced by the periodic boundary condition, which is suitable for the computation of $\hat{L}_{MQ}$. The upper wall is still diffusely reflective, but the lower walls now have two different configurations (as shown in Fig. 5):

(1) All the lower walls are diffusely reflective. This is referred to as the diffuse configuration.

(2) The lower horizontal and vertical walls are diffusely reflective, and the lower tilted walls are specularly reflective. This is referred to as the diffuse-specular configuration, the same as that adopted in Ref. [17].

Technically, these two configurations are compatible with the periodic boundary condition applied here, under which only the thermo-osmotic effect is attainable and the coefficient $\hat{L}_{MQ}$ can be computed. As to the configuration shown in Fig. 2(a), it is suitable for the application of pressure difference, under which the mechano-caloric effect coexists with the thermo-osmotic effect, and hence $\hat{L}_{QM}$ and $\hat{L}_{MQ}$ can be computed simultaneously to verify the reciprocal symmetry.

Figure 6 shows $\hat{L}_{MQ}$ as a function of $\tan\alpha$ for $L/H = 2$, $H_1/H = 1$, and $\mathrm{Kn} = 0.28$. The left panel in the figure is for the diffuse configuration, and the right panel is for the diffuse-specular

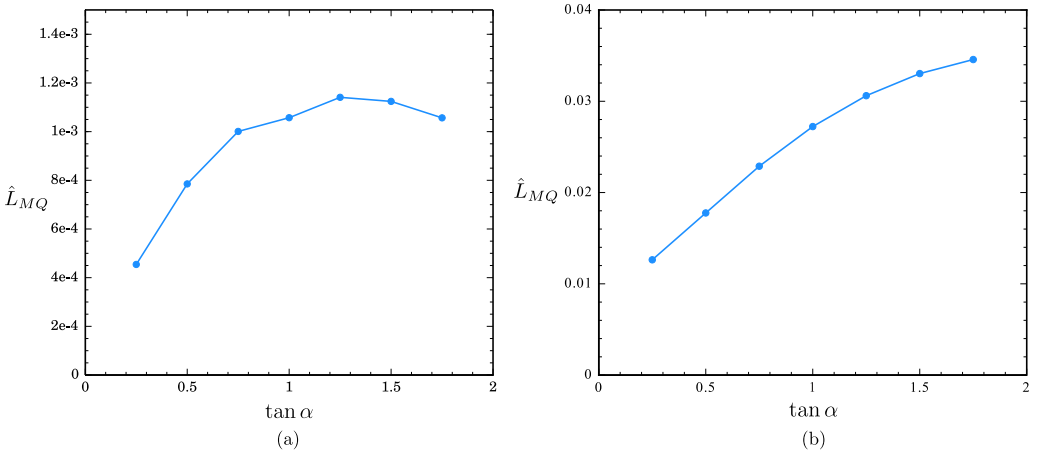

FIG. 6. $\hat{L}_{MQ}$ plotted as a function of $\tan\alpha$ for $L/H = 2$, $H_1/H = 1$, and $\mathrm{Kn} = 0.28$. (a) $\hat{L}_{MQ}$ in the diffuse configuration. (b) $\hat{L}_{MQ}$ in the diffuse-specular configuration.

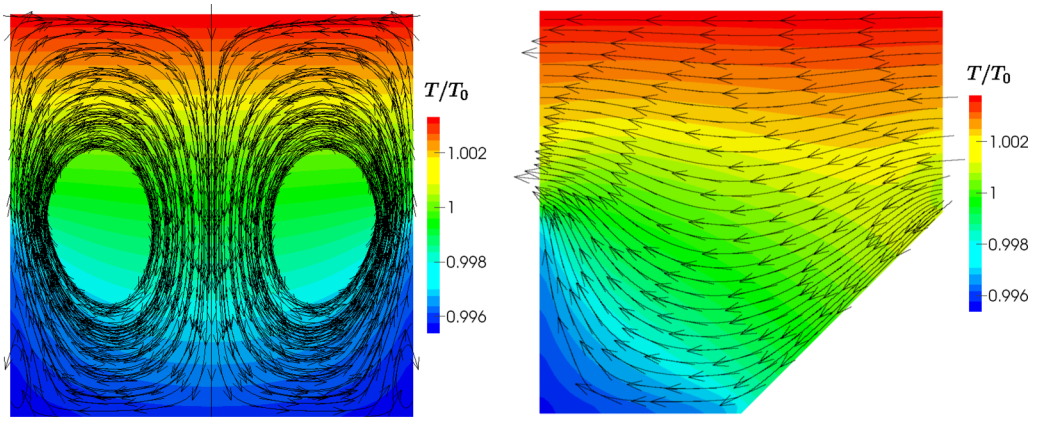

FIG. 7. The temperature distribution and streamlines plotted in one block with the periodic boundary condition. (a) The diffuse configuration with $\alpha = 0$. (b) A typical diffuse-specular configuration.

configuration. In the diffuse configuration, the thermally induced flows arise on both sides of the sharp edge and the net flow is consequently diminished [16]. This explains the very small magnitude of $\hat{L}_{MQ}$ in Fig. 6(a). In fact, if $\alpha = 0$, then there will be no net mass flow in the x direction because two identical vortices are formed between the "needles" as shown in Fig. 7(a). The optimal value of α (at which $\hat{L}_{MQ}$ is maximized) is approximately given by $\tan\alpha = 1.25$. In the diffuse-specular configuration, the thermally induced flow occurs only on the diffusely reflective surfaces, and therefore the net mass flow is much higher than that in the diffuse configuration. The temperature distribution and streamlines of a typical diffuse-specular configuration are shown in Fig. 7(b), and they are similar to the corresponding results in Ref. [17]. In this case, Fig. 6(b) shows $\hat{L}_{MQ}$ to be an increasing function of $\tan\alpha$. For L/H and H_1/H used here, $\tan\alpha$ varies between 0 and 2. At a larger α, the flow explores a smaller region between the vertical and tilted walls, with the streamlines showing less change in direction. This means the flow is less dissipated, and the thermo-osmotic effect is stronger.

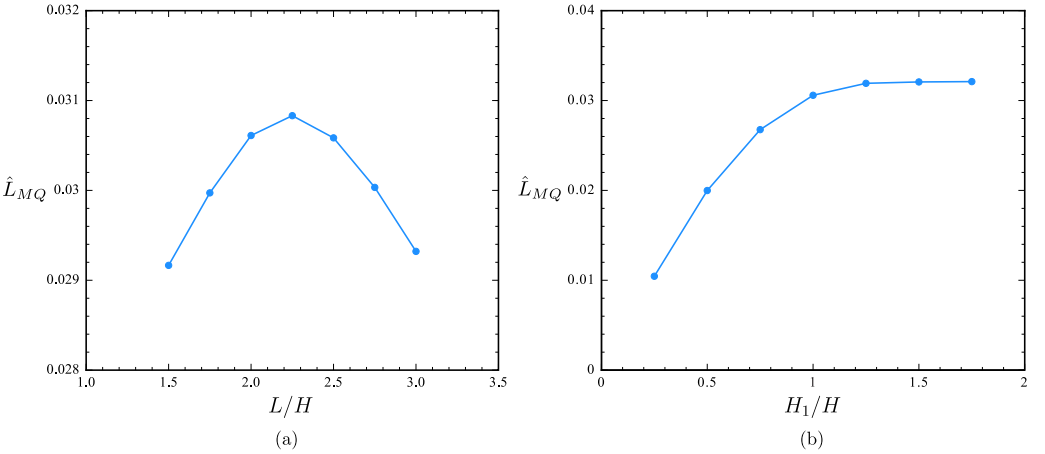

FIG. 8. $\hat{L}_{MQ}$ in the diffuse-specular configuration. (a) $\hat{L}_{MQ}$ plotted as a function of L/H for $\tan\alpha = 1.25$, $H_1/H = 1$, and $\mathrm{Kn} = 0.28$. (b) $\hat{L}_{MQ}$ plotted as a function of H_1/H for $\tan\alpha = 1.25$, $L/H = 2.5$, and $\mathrm{Kn} = 0.28$.

Now we focus on the diffuse-specular configuration. Figure 8(a) shows $\hat{L}_{MQ}$ as a function of L/H for $\tan\alpha = 1.25$, $H_1/H = 1$, and $\mathrm{Kn} = 0.28$. It is seen that $\hat{L}_{MQ}$ is maximized at $L/H \approx 2.25$. Here L/H can increase from 1.25 to ∞. When L/H is close to 1.25, the flow changes greatly in direction at the lower left corner, and hence the density of dissipation is large. On the other hand, when L/H is very large, the total dissipation is also large because of the large space involved. As a consequence, an optimal value of L/H is expected at which the total dissipation is minimized and $\hat{L}_{MQ}$ is maximized. Figure 8(b) shows the $\hat{L}_{MQ}$ as a function of H_1/H for $\tan\alpha = 1.25$, $L/H = 2.5$, and $\mathrm{Kn} = 0.28$. Here H_1/H varies between 0 and 2. It is seen that $\hat{L}_{MQ}$ is an increasing function of H_1/H and saturates at $H_1/H \approx 1.25$. This is expected because the thermally induced flow is appreciable only within a certain distance to the edge. For H_1 below this distance, $\hat{L}_{MQ}$ increases with the increasing H_1, while for H_1 above this distance, $\hat{L}_{MQ}$ saturates.

V. CONCLUDING REMARKS

The mechano-caloric effect and thermo-osmotic effect in a single-component gas not far from equilibrium have been investigated. The mechanisms for micro-channels with planar surfaces and ratchet surfaces have been analyzed. Numerical simulations have been performed to compute the off-diagonal kinetic coefficients for the cross coupling effects as a function of the Knudsen number. For channels with planar surfaces, our simulation results have been compared with the S-model solution of Chernyak *et al.* [24], showing good agreement for $0.1 < \mathrm{Kn} < 10$. For channels with ratchet surfaces, our simulations have been performed for both the slip and transition regimes. The theoretical prediction for micro-channels with ratchet surfaces in the slip regime, which gives $\overline{U} \propto \hat{L}_{MQ} \propto \mathrm{Kn}^C$, has been numerically checked, showing good agreement with our simulation results. It has also been shown that $\hat{L}_{MQ}$ and $\hat{L}_{QM}$ both exhibit their maxima at $\mathrm{Kn} \approx 0.28$ in the transition regime, as anticipated theoretically.

For both types of channels, our simulation results for the off-diagonal kinetic coefficients have confirmed Onsager's reciprocal relation. Given the fundamental importance of reciprocal symmetry in nonequilibrium thermodynamics, we want to point out that (i) our simulation geometry for channels of ratchet surfaces allows the coexistence of the mechano-caloric and thermo-osmotic effects, (ii) this coexistence makes the numerical verification of reciprocal symmetry possible, and (iii) this verification shows that thermodynamic consistency is ensured in our simulation approach based on the unified gas-kinetic scheme [18,19]. Here we remark that the reciprocal symmetry has been observed in the slip regime and beyond. This is physically acceptable because small pressure and temperature differences have been used in our simulations to ensure that dynamics is slow, and hence linear response is valid even if the Knudsen number is not very small.

Since micro-channels with ratchet surfaces have the potential to be an alternative configuration of Knudsen pump, a preliminary optimization study has been carried out for its geometry. Two different configurations have been used for this purpose: (i) the diffuse configuration in which all the lower walls are diffusely reflective, and (ii) the diffuse-specular configuration in which the lower horizontal and vertical walls are diffusely reflective and the lower tilted walls are specularly reflective. It turns out that the diffuse-specular configuration leads to a much stronger thermo-osmotic effect (by an order of magnitude). In particular, we have measured the off-diagonal coefficient $\hat{L}_{MQ}$ as a function of various geometrical parameters, and our results can be used to help optimize the pump design. We would like to point out that it is difficult to find a specularly reflective surface and hence the diffuse-specular configuration is mostly of theoretical interest at the moment. Alternative configurations with different combinations of wall boundary conditions, including adiabatic boundaries [27], are yet to be explored for the practical design of Knudsen pump.

ACKNOWLEDGMENT

This work is supported by Hong Kong RGC Grants No. HKUST604013 and No. C6004-14G.

APPENDIX: SIMULATION METHOD: UNIFIED GAS-KINETIC SCHEME

The unified gas-kinetic scheme (UGKS) is a multiscale simulation method based on the kinetic equation, which can be used for simulating flows of all Knudsen numbers [18,19]. Here we give a brief outline of the UGKS. For simplicity, the formulation is presented for one-dimensional space, but the extension to higher dimensional space is straightforward and has been given in detail in Ref. [19]. In our simulations, the two-dimensional version has been used.

The BGK-type equation in one spatial dimension without external force is given by

$$\frac{\partial f}{\partial t} + u\frac{\partial f}{\partial x} = Q(f), \quad Q(f) = \frac{f^+ - f}{\tau}, \tag{A1}$$

where $f(x,t,\mathbf{u})$ is the velocity distribution function at (x,t), $\mathbf{u} = (u,v,w)$ is the particle velocity, f^+ is the postcollision distribution function, and τ is the relaxation time. In the finite-volume framework, the evolution of the distribution function and conservative variables in the ith cell are given by

$$f_i^{n+1} = f_i^n - \frac{1}{\Delta x}\int_{t^n}^{t^{n+1}} u(f_{i+1/2} - f_{i-1/2})\,dt + \frac{\Delta t}{2}\left(Q_i^n + Q_i^{n+1}\right) \tag{A2}$$

and

$$\mathbf{W}_i^{n+1} = \mathbf{W}_i^n - \frac{1}{\Delta x}\int_{t^n}^{t^{n+1}}\int \psi u(f_{i+1/2} - f_{i-1/2})\,d\mathbf{u}\,dt, \tag{A3}$$

where $\mathbf{W} = (\rho,\rho U,\rho E)^T$, $\psi = (1,u,\mathbf{u}^2/2)^T$, U is the macroscopic velocity, E is the total energy density, and $d\mathbf{u} = du\,dv\,dw$.

The construction of the interface flux is the key to UGKS. Assuming an interface is located at $x = 0$, the accurate time evolution of the distribution function at the interface from $t^n = 0$ to $t^{n+1} = \Delta t$ is described by the solution of the BGK-type equation along the characteristics,

$$f(0,t,\mathbf{u}) = \frac{1}{\tau}\int_0^t f^+(-u(t-t'),t',\mathbf{u})e^{-(t-t')/\tau}\,dt' + e^{-t/\tau}f_0(-ut,\mathbf{u}), \tag{A4}$$

where f_0 is the initial distribution function at $t = 0$. Here f_0 is assumed to be linearly distributed within each cell and discontinuous at the interface, given by

$$f_0 = \left(f_0^L + xf_x^L\right)(1 - H[x]) + \left(f_0^R + xf_x^R\right)H[x], \tag{A5}$$

where f_0^L and f_0^R are the reconstructed distribution functions at both sides of the cell interface, f_x^L and f_x^R are the corresponding derivatives, and $H[x]$ is the Heaviside function. The postcollision term f^+ is approximated by the first-order Taylor expansion on both sides of the interface, given by

$$f^+ = f_0^+ + g_0[(1 - H[x])a^Lx + H[x]a^Rx + At], \tag{A6}$$

where g_0 is the Maxwell distribution which is uniquely determined by $\mathbf{W}_0$,

$$\mathbf{W}_0 = \int \left(f_0^L H[u] + f_0^R(1 - H[u])\right)\psi\,d\mathbf{u}. \tag{A7}$$

The coefficients a^L, a^R, and A are computed via the partial derivatives of the conservative variables at $(x,t) = (0,0)$, for example,

$$a^L = \frac{1}{g_0}\left(\frac{\partial g_0}{\partial \mathbf{W}_0}\right)\mathbf{W}_x^L \approx \frac{1}{g_0}\left(\frac{\partial g_0}{\partial \mathbf{W}_0}\right)\frac{\mathbf{W}^L - \mathbf{W}_0}{x^L}, \tag{A8}$$

where $\mathbf{W}^L$ is the conservative variables at the left cell, and x^L is the coordinate of the left cell center. The time derivative part A is computed via

$$\mathbf{W}_t = -\int \{a^L H[u] + a^R(1 - H[u])\} u g_0 \psi \, d\mathbf{u}. \tag{A9}$$

In the present work, f^+ takes the form from the BGK-Shakhov model [28] to result in a realistic Prandtl number, and the relaxation time is $\tau = \mu/p$.

The method outlined above is mainly for the calculation of the flux across the inner cell interface. For the cell interface at the boundary, the procedure needs to be modified according to the boundary conditions. The UGKS method can handle a variety of boundary conditions, such as diffuse boundary, specular boundary, and pressure inlet and outlet. Their implementation is similar to that in other simulation methods for solving the kinetic equations.

[1] L. Onsager, Reciprocal Relations in Irreversible Processes. I. Phys. Rev. **37**, 405 (1931).

[2] L. Onsager, Reciprocal Relations in Irreversible Processes. II. Phys. Rev. **38**, 2265 (1931).

[3] G. M. Kremer, *An Introduction to the Boltzmann Equation and Transport Processes in Gases* (Springer, Berlin, 2010), pp. 1–310.

[4] L. Waldmann, Non-equilibrium thermodynamics of boundary conditions, Z. Naturforsch. A **22**, 1269 (1967).

[5] Y. Sone, *Kinetic Theory and Fluid Dynamics* (Birkhäuser, Boston, 2002), pp. 1–353.

[6] K. Aoki, P. Degond, L. Mieussens, M. Nishioka, and S. Takata, Numerical simulation of a Knudsen pump using the effect of curvature of the channel, in *Rarefied Gas Dynamics*, edited by M. S. Ivanov and A. K. Rebrov (Siberian Branch of the Russian Academy of Sciences, Novosibirsk, Russia, 2007), pp. 1079–1084.

[7] S. R. de Groot and P. Mazur, *Non-Equilibrium Thermodynamics* (Dover, New York, 1984), pp. 1–510.

[8] S. K. Loyalka, Kinetic theory of thermal transpiration and mechanocaloric effect. I, J. Chem. Phys. **55**, 4497 (1971).

[9] S. K. Loyalka, Kinetic theory of thermal transpiration and mechanocaloric effect. II, J. Chem. Phys. **63**, 4054 (1975).

[10] F. Sharipov, Onsager-Casimir reciprocal relations based on the Boltzmann equation and gas-surface interaction: Single gas, Phys. Rev. E **73**, 026110 (2006).

[11] Fe. Sharipov and V. Seleznev, Data on internal rarefied gas flows, J. Phys. Chem. Ref. Data **27**, 657 (1998).

[12] F. Sharipov, Non-isothermal gas flow through rectangular microchannels, J. Micromech. Microeng. **9**, 394 (1999).

[13] I. Graur and F. Sharipov, Non-isothermal flow of rarefied gas through a long pipe with elliptic cross section, Microfluid. Nanofluid. **6**, 267 (2009).

[14] K. Ritos, Y. Lihnaropoulos, S. Naris, and D. Valougeorgis, Pressure- and temperature-driven flow through triangular and trapezoidal microchannels, Heat Transfer Eng. **32**, 1101 (2011).

[15] A. Würger, Leidenfrost Gas Ratchets Driven by Thermal Creep, Phys. Rev. Lett. **107**, 164502 (2011).

[16] S. Hardt, S. Tiwari, and T. Baier, Thermally driven flows between a Leidenfrost solid and a ratchet surface, Phys. Rev. E **87**, 063015 (2013).

[17] A. A. Donkov, S. Tiwari, T. Liang, S. Hardt, A. Klar, and W. Ye, Momentum and mass fluxes in a gas confined between periodically structured surfaces at different temperatures, Phys. Rev. E **84**, 016304 (2011).

[18] Kun Xu and Juan-Chen Huang, A unified gas-kinetic scheme for continuum and rarefied flows, J. Comput. Phys. **229**, 7747 (2010).

[19] J.-C. Huang, K. Xu, and P. Yu, A unified gas-kinetic scheme for continuum and rarefied flows II: Multi-dimensional cases, Commun. Comput. Phys. **12**, 662 (2012).

[20] I. Gyarmati, *Non-equilibrium Thermodynamics* (Springer, Berlin, 1970), pp. 1–184.

[21] F. Sharipov, Onsager-Casimir reciprocity relations for open gaseous systems at arbitrary rarefaction I. General theory for single gas, Physica A **203**, 437 (1994).
[22] F. Sharipov, Onsager-Casimir reciprocity relations for open gaseous systems at arbitrary rarefraction II. Application of the theory for single gas, Physica A **203**, 457 (1994).
[23] Ching Shen, *Rarefied Gas Dynamics* (Springer, Berlin, 2005), p. 421.
[24] V. G. Chernyak, V. V. Kalinin, and P. E. Suetin, Theory of nonisothermal gas motion in a plane channel, J. Eng. Phys. **36**, 696 (1979).
[25] T. Ohwada, Y. Sone, and K. Aoki, Numerical analysis of the Poiseuille and thermal transpiration flows between two parallel plates on the basis of the Boltzmann equation for hard-sphere molecules, Phys. Fluids A **1**, 2042 (1989).
[26] C. Cercignani, *The Boltzmann Equation and Its Applications* (Springer, New York, 1988), pp. 1–456.
[27] A. Mohammadzadeh, A. Rana, and H. Struchtrup, DSMC and R13 modeling of the adiabatic surface, Int. J. Therm. Sci. **101**, 9 (2016).
[28] E. M. Shakhov, Generalization of the Krook kinetic relaxation equation, Fluid. Dyn. **3**, 95 (1972).